Cell Reports, Volume *31*

Supplemental Information

Molecular Analysis of Clinically Defined Subsets of High-Grade Serous Ovarian Cancer

Sanghoon Lee, Li Zhao, Christine Rojas, Nicholas W. Bateman, Hui Yao, Olivia D. Lara, Joseph Celestino, Margaret B. Morgan, Tri V. Nguyen, Kelly A. Conrads, Kelly M. Rangel, Robert L. Dood, Richard A. Hajek, Gloria L. Fawcett, Randy A. Chu, Katlin Wilson, Jeremy L. Loffredo, Coralie Viollet, Amir A. Jazaeri, Clifton L. Dalgard, Xizeng Mao, Xingzhi Song, Ming Zhou, Brian L. Hood, Nirad Banskota, Matthew D. Wilkerson, Jerez Te, Anthony R. Soltis, Kristin Roman, Andrew Dunn, David Cordover, Agda Karina Eterovic, Jinsong Liu, Jared K. Burks, Keith A. Baggerly, Nicole D. Fleming, Karen H. Lu, Shannon N. Westin, Robert L. Coleman, Gordon B. Mills, Yovanni Casablanca, Jianhua Zhang, Thomas P. Conrads, George L. Maxwell, P. Andrew Futreal, and Anil K. Sood

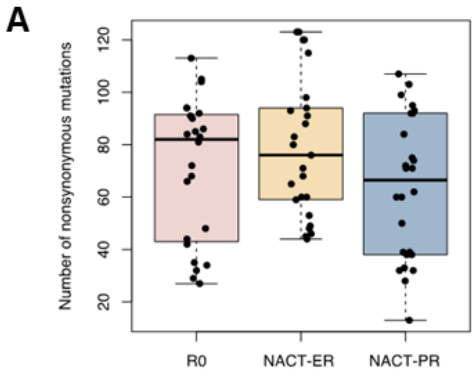

Group	p-values
R0 vs NACT-PR	0.6454
R0 vs NACT-ER	0.1959
NACT-ER vs NACT-PR	0.0546
R0 vs NACT-ER/PR	0.6201

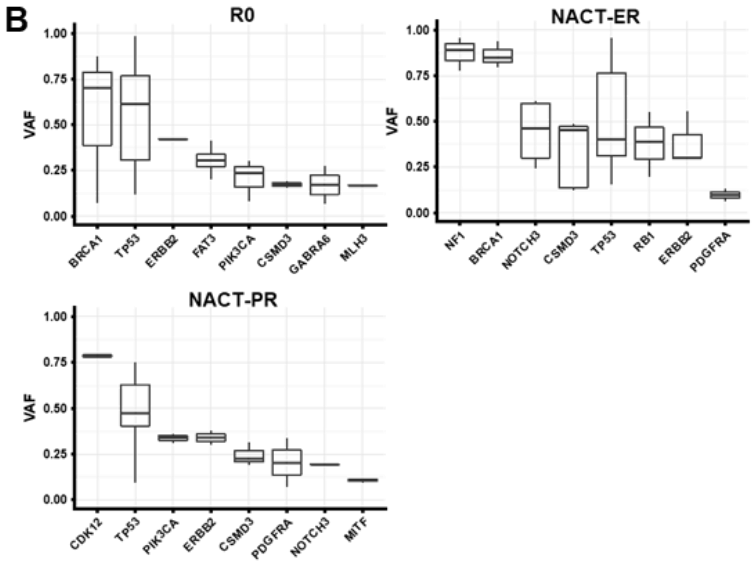

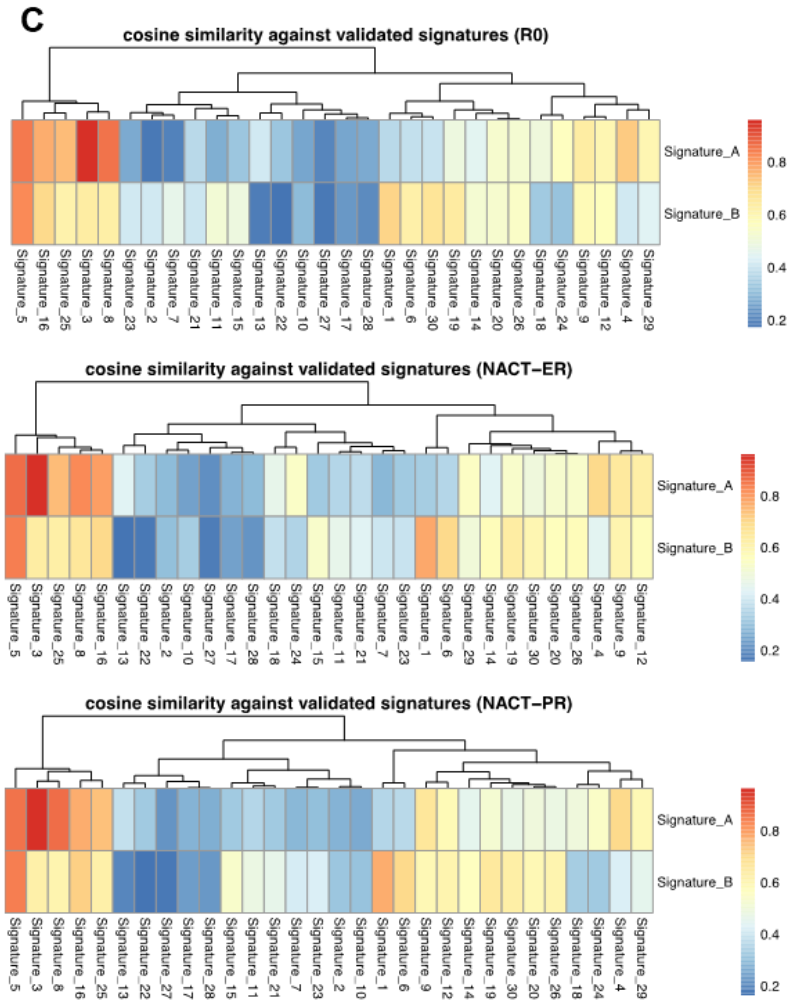

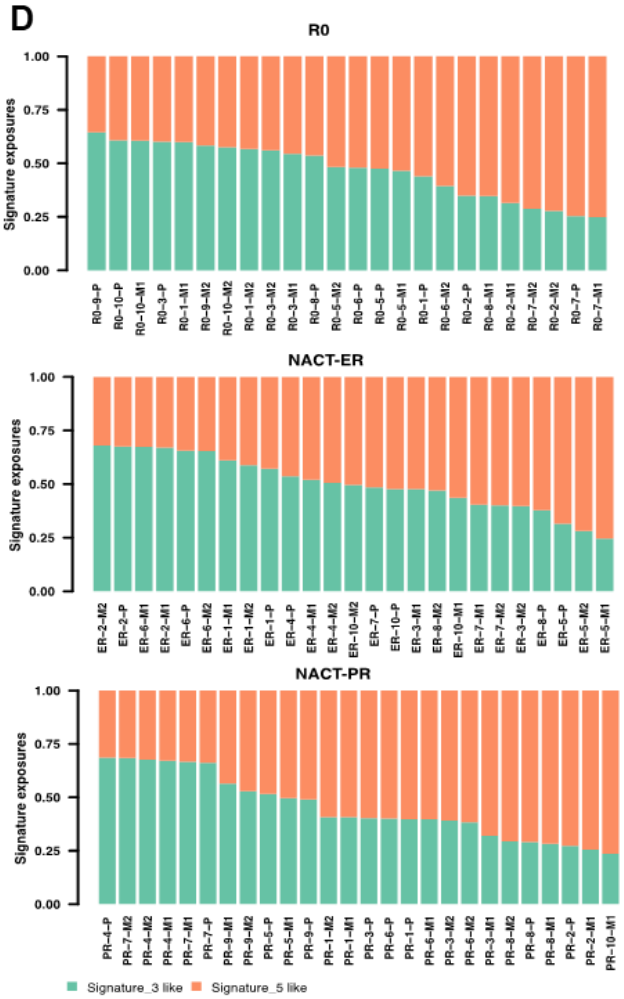

Figure S1. Somatic mutations by WGS, Related to Figure 2, Related to Figure 2. (A) Boxplot showing numbers of non-synonymous mutations. The average numbers were 81 in the R0, 78 in the NACT-ER and 67 in the NACT-PR groups. The p-value table shows all the comparisons between groups. (B) Boxplots showing the distribution of variant allele frequencies (VAFs) of somatic mutations identified in the R0 (top left), NACT-ER (top right) and NACT-PR (bottom) groups. (C) Mutation signatures identified from all somatic mutations. Two signatures, 3 and 5, from the 30 validated signatures in the COSMIC database were identified as enriched in our cohort. (D) The contribution of each sample to the two mutation signatures: Signature_3 like and Signature_5 like.

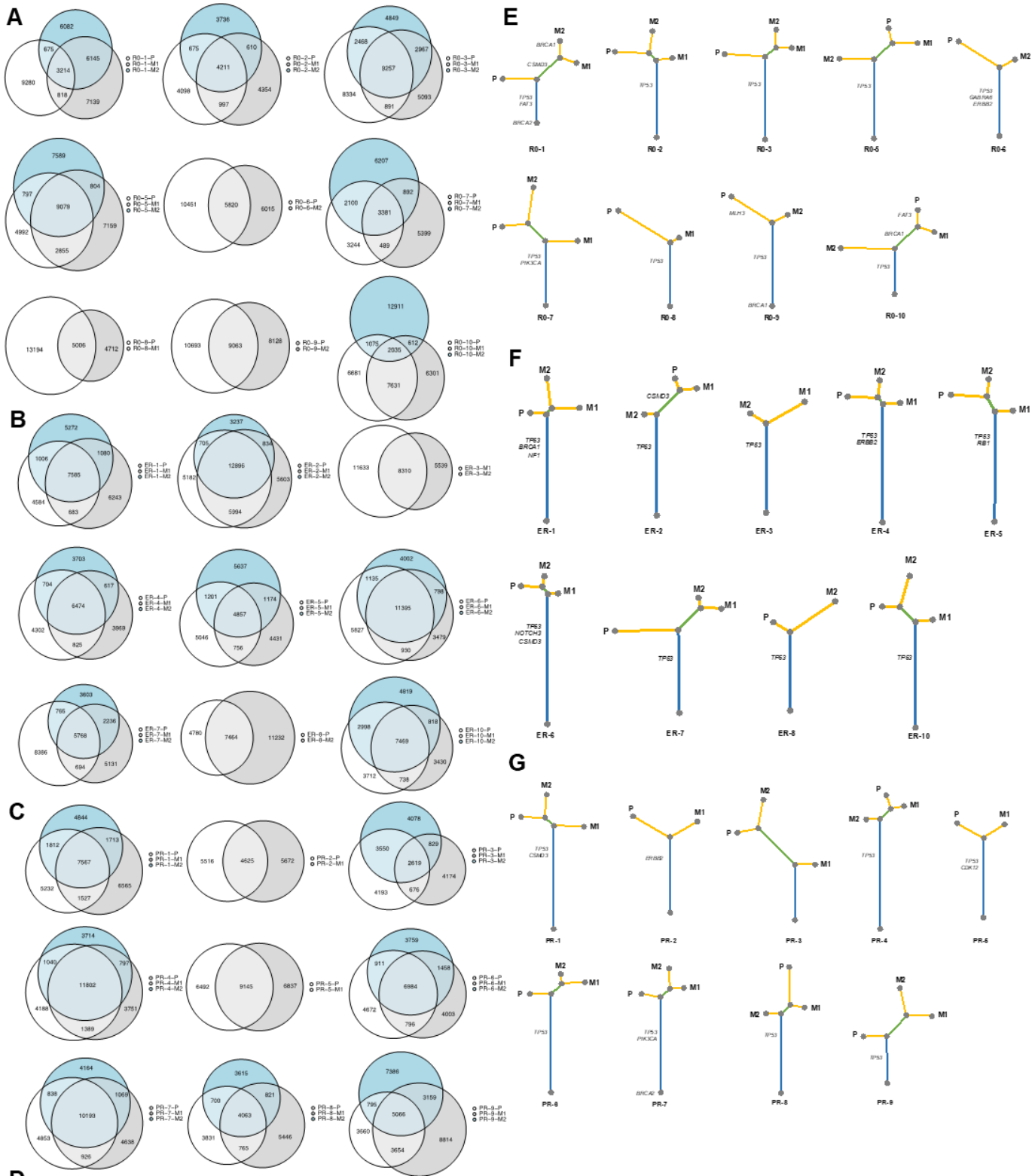

	p-values
R0 vs NACT-PR	0.642
R0 vs NACT-ER	0.781
NACT-ER vs NACT-PR	0.936
R0 vs NACT-ER/PR	0.646

	p-values
R0 vs NACT-PR	0.436
R0 vs NACT-ER	0.971
NACT-ER vs NACT-PR	0.481
R0 vs NACT-ER/PR	0.681

	p-values
R0 vs NACT-PR	0.424
R0 vs NACT-ER	1.000
NACT-ER vs NACT-PR	0.444
R0 vs NACT-ER/PR	0.641

Figure S2. Intra-patient heterogeneity, clonal analysis and phylogenetic trees of cancer progression of patients in the R0, NACT-ER and NACT-PR groups, Related to Figure 2. (A-C) Venn diagrams of all the somatic mutations identified in primary and distant metastatic sites by patient in the R0 (A), NACT-ER (B) and NACT-PR (C) groups. (D) Boxplots showing clonal analysis, (Left) the number of clones, (Middle) the proportion of mutations belonging to major clones and (Right) the cellular prevalence of major clones. (E-G) Phylogenetic tree of the samples constructed with non-silent mutations. The branch lengths are in proportion to the number of non-silent mutations, including SNVs and Indels. GL: Germline. Ovarian cancer-related mutations are marked on the tree in the R0 (E), NACT-ER (F) and NACT-PR (G) groups.

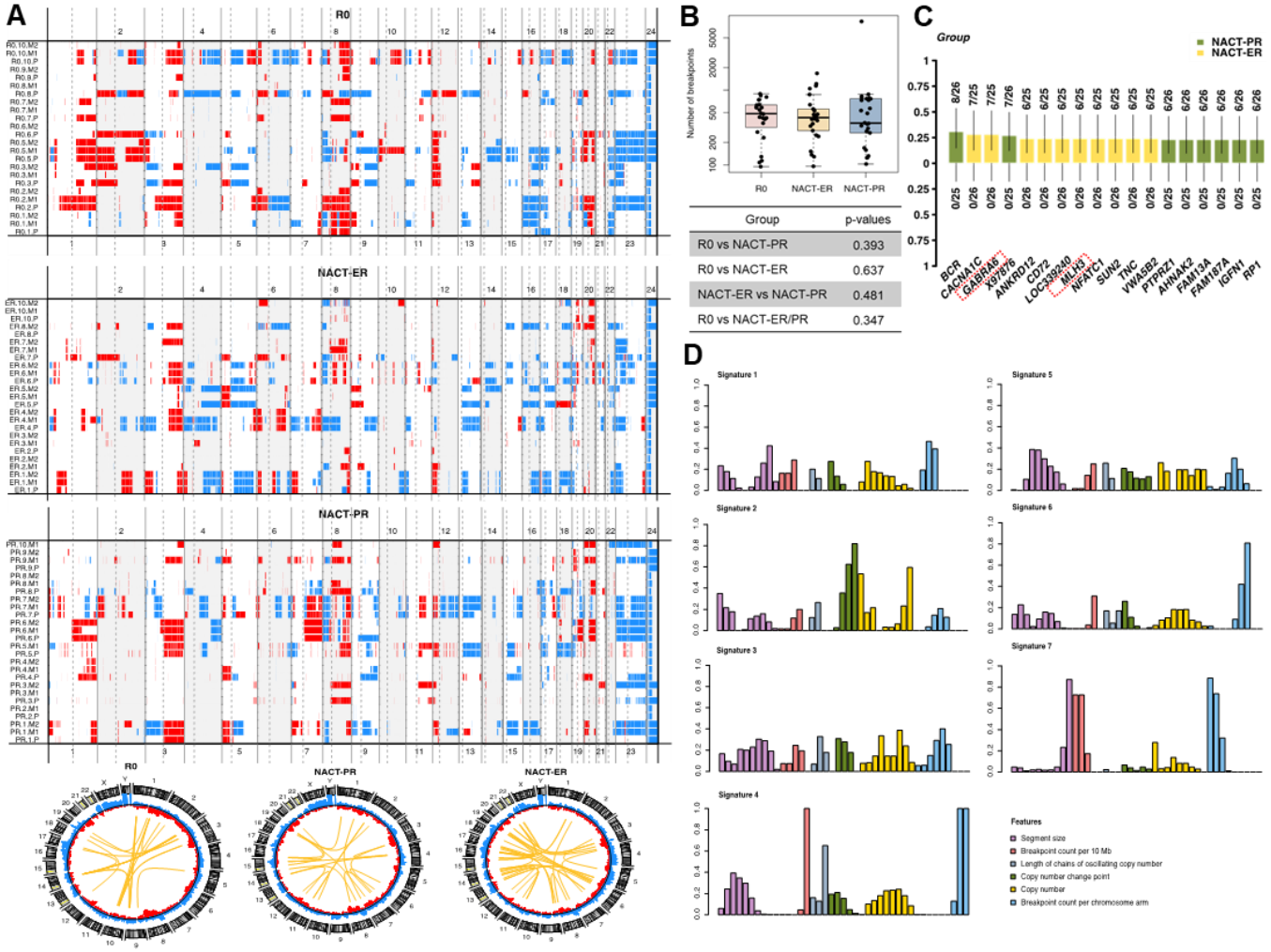

Group	p-values
R0 vs NACT-PR	0.393
R0 vs NACT-ER	0.637
NACT-ER vs NACT-PR	0.481
R0 vs NACT-ER/PR	0.347

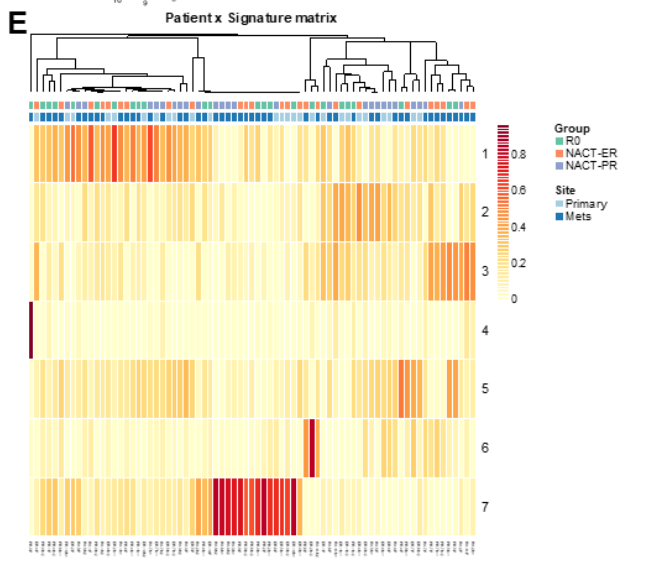

H

Group	Gene1	Gene2	Frame methods	No. of samples
R0	ARID1A	ZDHHC18	OutFrame:3bd,3bs,3lp	3
	ATP1B2	TP53	Head2Head:2bd,1bs,2lp	2
	CTNNB1	PTPN23	Head2Head:1bd,1bs,1lp	1
	RNF135	NF1	InFrame:1bd,1bs,1lp	1
	CDK12	ZPBP2	Tail2Tail:2bd,2lp	2
	SPATA5	ERBB2	OutFrame:1bd,2lp	2
	CSMD3	COLEC10	Head2Head:1bd,1lp	1
NACT-ER	NTN1	TP53	CD-UTR5:3bd,3bs,3lp	3
	RP11-360P21.2	PIK3CA	Tail2Tail:3bd,3bs,3lp	3
	AC079807.4	MSH2	UTR-CD:2bd,2bs,2lp	2
	CDH3	AKT2	InFrame:2bd,2bs,2lp	2
	LIN54	CDK12	Tail2Tail:1bd|UTR5-CD:1bs,1lp	3
	MYLK	CSMD3	UTR5-CD:1bd,1bs,1lp	1
	BRCA1	CASC15	CD-UTR:2bs,2lp	2
	IQCB1	MSH2	InFrame:1bs,1lp	2
	JAG2	PACS2	CD-UTR5:1bd,1lp	1
	JAG2	BRF1	CD-UTR5:1bd,1lp	1
NACT-PR	NF1	NSRP1	OutFrame:3bd,3bs,3lp	3
	CHEK2	TTC28	OutFrame:3bd,3bs,3lp	3
	PPIE	CCNE1	UTR5-CD:2bd,2bs,3lp	3
	EPCAM	MSH2	Tail2Tail:1bd|UTR-CD:2bs,2lp|UTR5-CD:2bd	3
	PTPRD	CDKN2B-AS1	Tail2Tail:2bd,2bs,2lp	2
	CTNNB1	ULK4	Head2Head:1bd,1bs,1lp	1
	FAT3	SLC22A6	CD-UTR3:2bd,3lp	3
	EIF2B5	JAG2	InFrame:2bs,2lp	2
	RN7SKP119	MSH2	UTR-CD:2bs,2lp	2

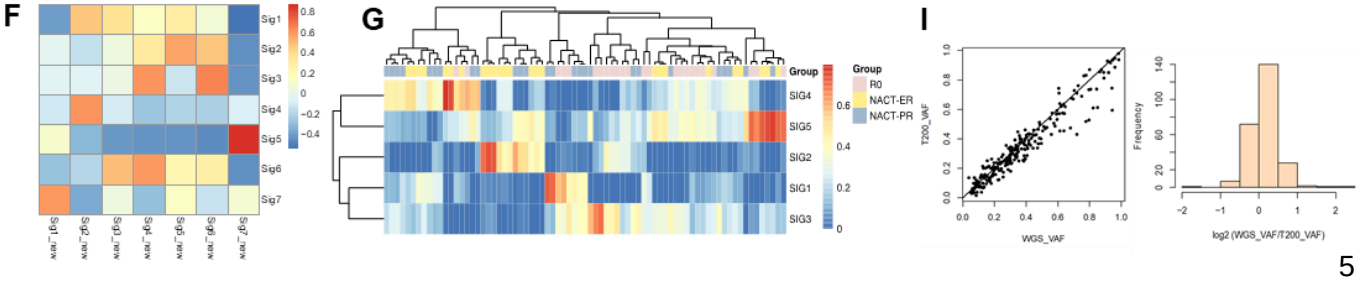

Figure S3. Copy number profiles, the load of copy number variations, copy number signatures and structure variations in all patient groups, Related to Figure 2. (A) Copy number profiles across the entire genome. Top: Copy number variations of all samples. Red indicates copy gains, and blue indicates copy losses. Samples from the same patients are next to each other. Bottom: Circle plots of the frequencies of copy gains/losses on each chromosome, and the yellow lines indicate inter-chromosomal translocations. (B) Boxplot showing the number of copy number breakpoints calculated. The median numbers of breakpoints per sample were 485 in the R0 group, 429 in the NACT-ER group and 363 in the NACT-PR group. (C) Shown are the enriched abnormalities, including somatic mutations and CNVs, with a significant p-value <0.05 in the comparison between NACT-ER (n=25) and NACT-PR (n=26) groups. The y-axis represents the proportion of patient samples carrying the mutation in the corresponding genes, the numbers labeled in the graph indicate the number of mutated samples/total number of samples in the corresponding genes. The red dot box in the x-axis represents ovarian cancer-related genes. (D) Seven copy number signatures are identified in our patient cohort. (E) Heatmap of the signature scores based on the identified copy number signatures for each patient. (F) the similarity ranging from 0 to 1 between the copy number signatures previously reported in high-grade serous ovarian cancer (Sig1 to Sig7) and the ones identified in our patient cohort (Sig1_new to Sig7_new). (G) Signature scores are calculated based on structure variations identified in each patient. The heatmap represents the cluster of signature scores across all patients. (H) Structure variations are identified in ovarian cancer associated genes. Three algorithms were used to detect structure variations, including brass (bs), breakdancer (bd) and lumpy (lp). (I) Left, scatterplot of VAFs of shared somatic mutations detected by WGS and T200 sequencing. Pearson correlation r=0.963, and Spearman correlation r=0.964. Right, histogram showing the log2 ratio of VAF in WGS and VAF in T200 sequencing.

A

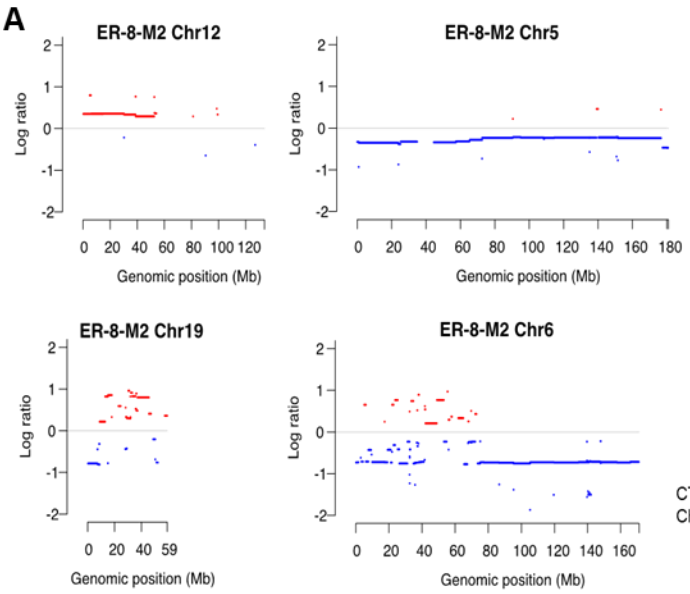

CTLP detected on Chr19 and Chr6

B

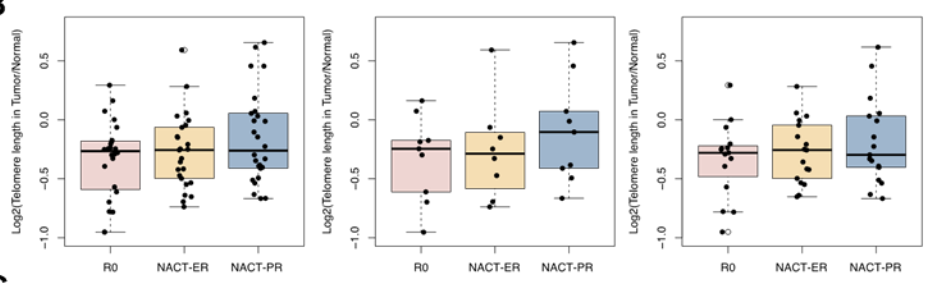

	Overall	Primary	Mets
R0 *vs* NACT-ER/PR	0.404	0.634	0.512
NACT-ER *vs* NACT-PR	0.335	0.423	0.610
R0 *vs* NACT-PR	0.284	0.436	0.478
R0 *vs* NACT-ER	0.729	1.000	0.682

C

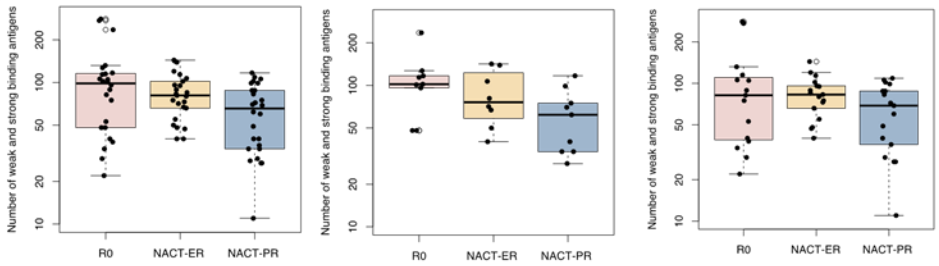

	Overall	Primary	Mets
R0 *vs* NACT-ER/PR	0.105	0.089	0.610
NACT-ER *vs* NACT-PR	0.033	0.148	0.134
R0 *vs* NACT-PR	0.023	0.030	0.265
R0 *vs* NACT-ER	0.617	0.531	0.835

D

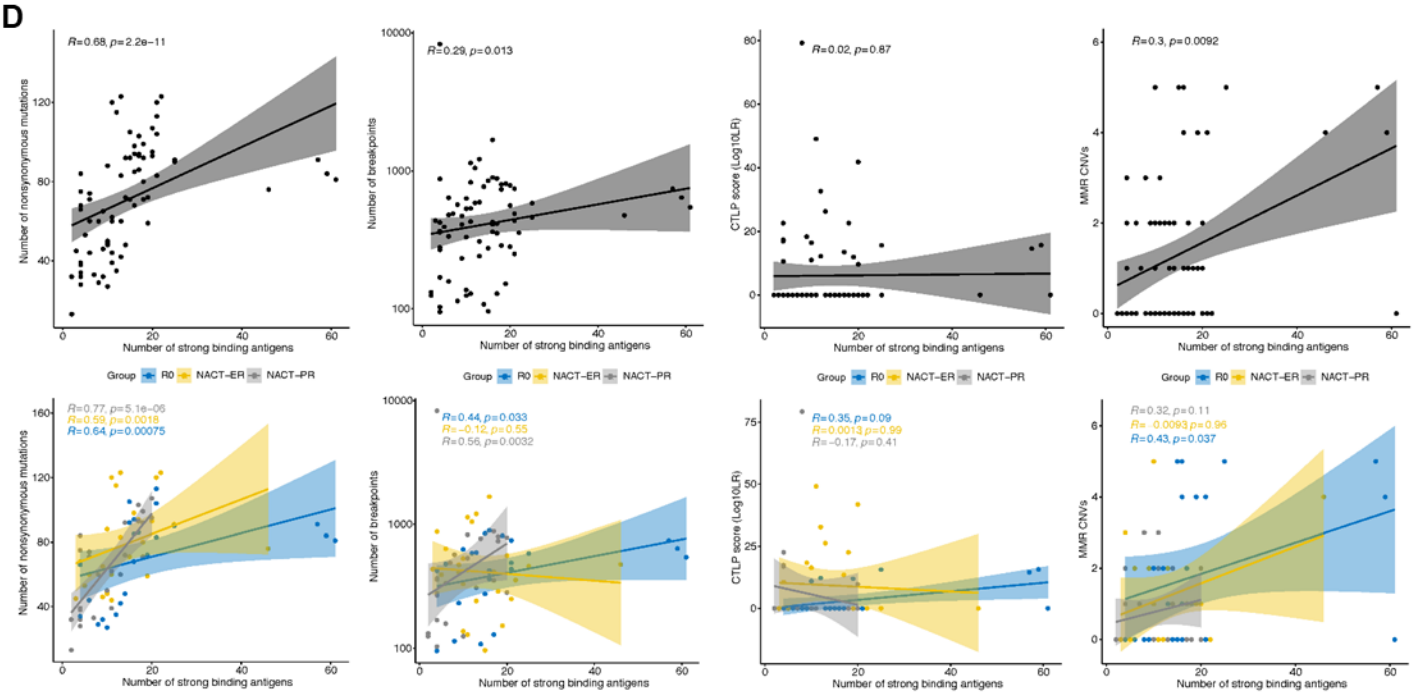

Figure S4. Chromothripsis-like patterns (CTLPs), telomere length (TL) ratios and the number of strong and weak binding antigens in patient groups, Related to Figure 3. (A) Examples of non-CLP (top) and CLP (bottom). In sample ER-8-M2, CTLPs were detected on chr6 and chr19. (B) The distribution of TL ratios (tumor/normal) in all samples (left), primary tumors (middle) and distant metastasis tumors (right). (C) Boxplots showing the number of antigens in all samples (left), primary tumors (middle) and distant metastasis tumors (right). These neoantigens show weak and strong binding in mutant, but not in original wild-type sequences. (D) The correlations between the neoantigen level and other features including mutation loads, CNV loads, CTLPs, and mismatch repair (MMR) CNVs.

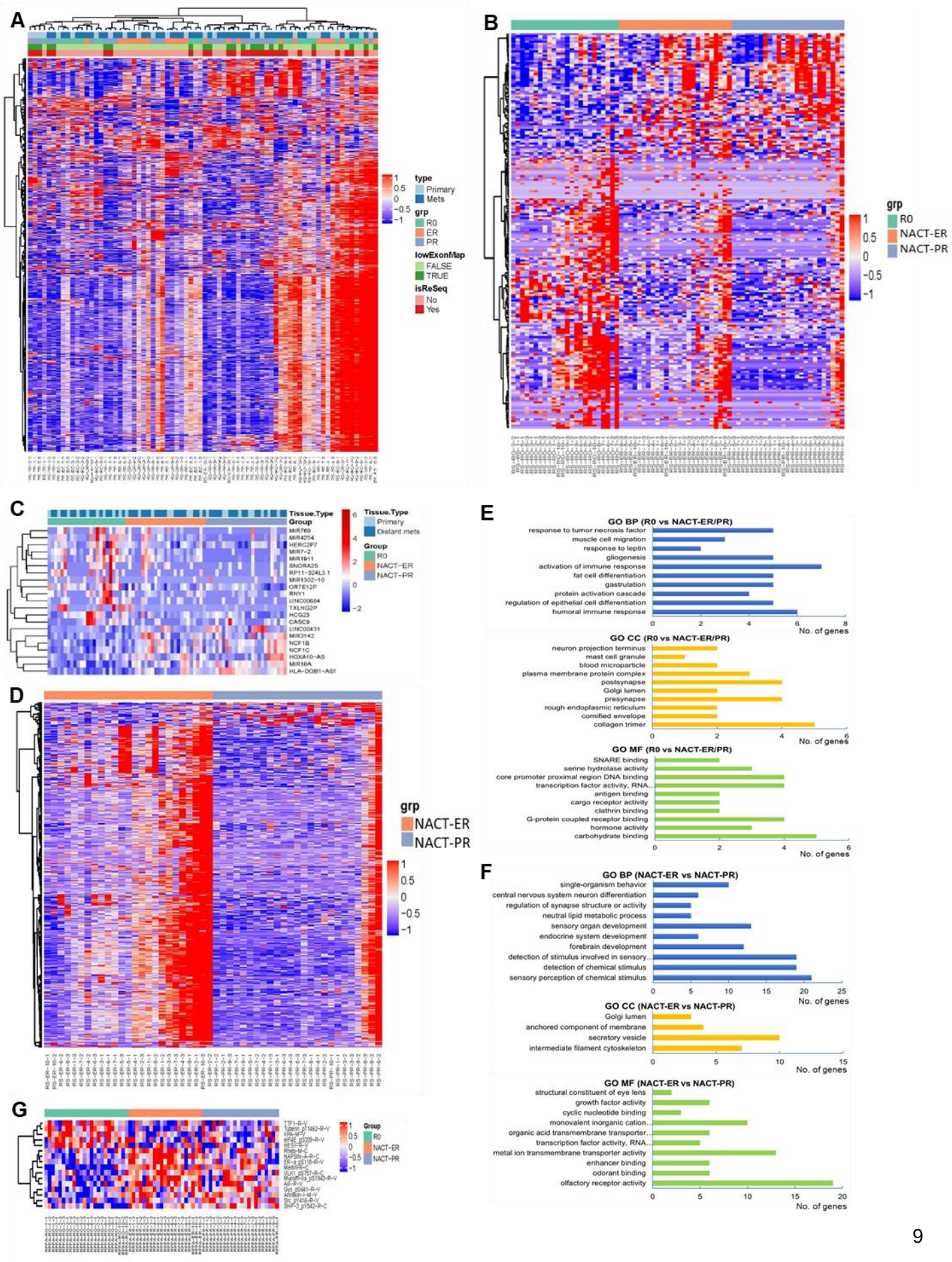
A
type
Primary
Mets
grp
R0
ER
PR
lowExonMap
FALSE
TRUE
isReSeq
No
Yes
B
grp
R0
NACT-ER
NACT-PR
C
Tissue.Type
Primary
Distant mets
Group
R0
NACT-ER
NACT-PR
MIR769
MIR4254
HERC2P7
MIR7-2
MIR1911
SNORA25
RP11-324L3.1
MIR1302-10
OR7E12P
RNY1
LINC00684
TXLNG2P
HCG23
CASC9
LINC00431
MIR3142
NCF1B
NCF1C
HOXA10-AS
MIR10A
HLA-DOB1-AS1
D
grp
NACT-ER
NACT-PR
E
GO BP (R0 vs NACT-ER/PR)
response to tumor necrosis factor
muscle cell migration
response to leptin
gliogenesis
activation of immune response
fat cell differentiation
gastrulation
protein activation cascade
regulation of epithelial cell differentiation
humoral immune response
No. of genes
GO CC (R0 vs NACT-ER/PR)
neuron projection terminus
mast cell granule
blood microparticle
plasma membrane protein complex
postsynapse
Golgi lumen
presynapse
rough endoplasmic reticulum
cornified envelope
collagen trimer
No. of genes
GO MF (R0 vs NACT-ER/PR)
SNARE binding
serine hydrolase activity
core promoter proximal region DNA binding
transcription factor activity, RNA...
antigen binding
cargo receptor activity
clathrin binding
G-protein coupled receptor binding
hormone activity
carbohydrate binding
No. of genes
F
GO BP (NACT-ER vs NACT-PR)
single-organism behavior
central nervous system neuron differentiation
regulation of synapse structure or activity
neutral lipid metabolic process
sensory organ development
endocrine system development
forebrain development
detection of stimulus involved in sensory...
detection of chemical stimulus
sensory perception of chemical stimulus
No. of genes
GO CC (NACT-ER vs NACT-PR)
Golgi lumen
anchored component of membrane
secretory vesicle
intermediate filament cytoskeleton
No. of genes
GO MF (NACT-ER vs NACT-PR)
structural constituent of eye lens
growth factor activity
cyclic nucleotide binding
monovalent inorganic cation...
organic acid transmembrane transporter...
transcription factor activity, RNA...
metal ion transmembrane transporter activity
enhancer binding
odorant binding
olfactory receptor activity
No. of genes
G
Group
R0
NACT-ER
NACT-PR

Figure S5. Differentially expressed genes (DEGs) identified by RNA-seq and RPPA in R0, NACT-ER and NACT-PR groups, Related to Figure 4. (A) Heatmap depicting the 3000 most variable genes based on RNA-seq. Rows indicate normalized gene expression level, and columns indicate samples. (B) Heatmap of The R0 group had significant 6 DEGs between the R0 and NACT-ER/PR groups, identified by RNA-seq. (C) Heatmap of differentially expressed ncRNA genes in the R0 versus NACT-ER and -PR groups, identified by RNA-seq. (D) Heatmap of 693 DEGs in the NACT-ER *versus* NACT-PR groups. (E-F) Significantly enriched GO terms BP, CC and MF in the R0 *versus* NACT-ER/PR groups (E), and NACT-ER *versus* NACT-PR groups (F). The x-axis represents the number of DEGs for each GO term category, and the y-axis represents the GO term category including BP, CC and MF. (G) Heatmap of 16 differentially expressed proteins between the R0 and the NACT-ER and -PR groups, identified by RPPA; a non-supervised clustering analysis was performed based on 297 protein expression levels from 67 tumor samples with a high level of tumor purity from across patient groups: 24 for the R0 group, 21 for the NACT-ER group and 22 for the NACT-PR group. Sixteen proteins were identified to be differentially expressed between the R0 and NACT-ER and -PR groups with an FDR < 0.15, and AMPK and SMAD3, were differentially upregulated in the NACT-ER compared to the NACT-PR group (FDR < 0.15) (data not shown).

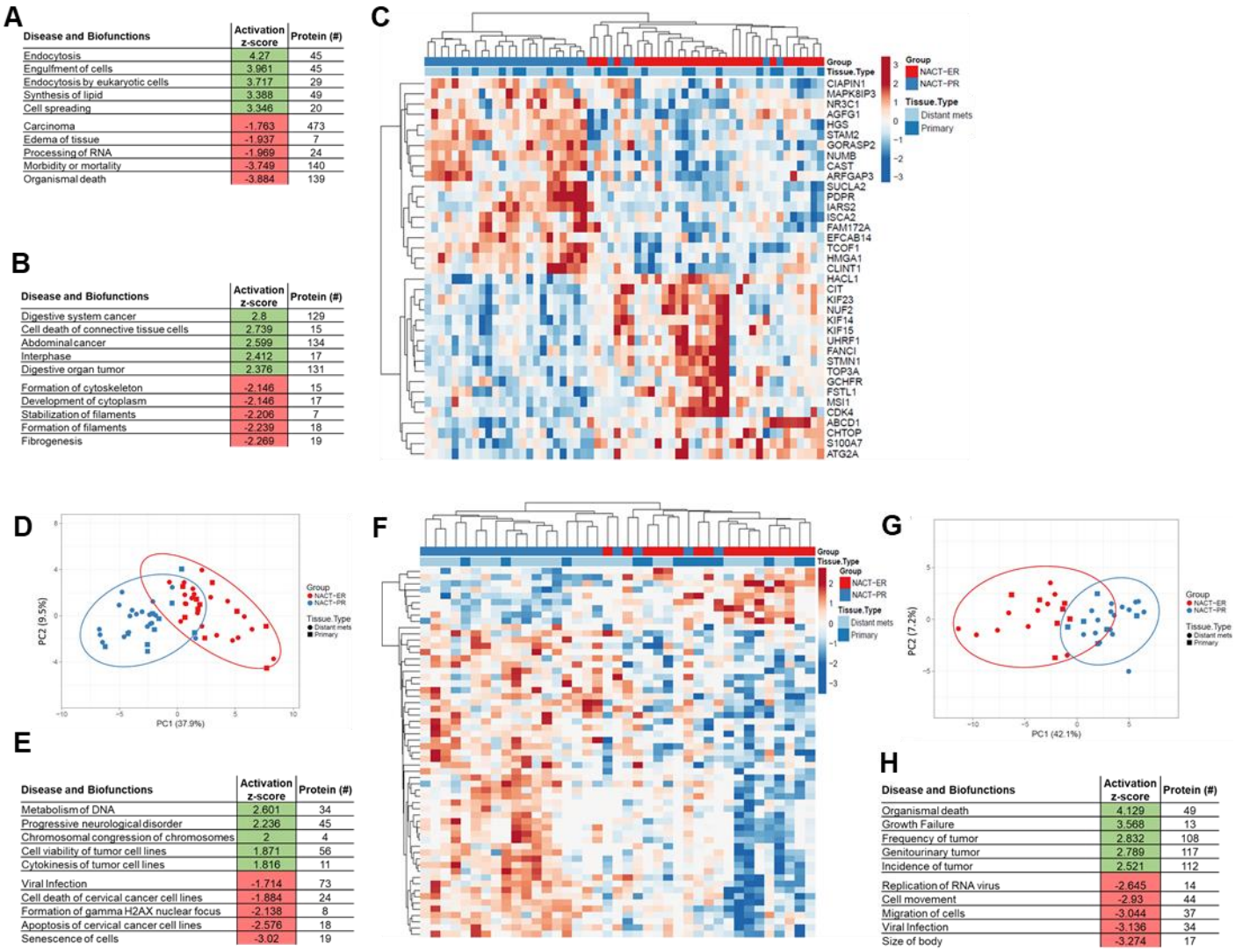

Figure S6. Differentially expressed genes (DEGs) identified by proteomics and principle component and pathway analyses of protein alterations in groups, Related to Figure 4. (A) Top pathways predicted to be activated (z-score >1) or inhibited (z-score <-1) inferred from 506 significant protein alterations between NACT-ER (n=30)/ PR (n=29) and R0 (n=28) patients. (B) Top pathways predicted to be activated (z-score >1) or inhibited (z-score <-1) inferred from 173 significant phosphosite alterations between NACT-ER (n=17)/ PR (n=22) and R0 (n=27) patients. (C) Differential analyses revealed 37 proteins significantly altered (adj. p-value <0.05) between NACT-ER (n=30) and NACT-PR (n=29) patients. Heatmap reflects clusters assembled

by Euclidean distance and average linkage of significant protein abundance trends. (D) Principle component analyses revealed 37 proteins significantly altered (adj. $p<0.05$) between NACT-ER (n=30) and NACT-PR (n=29) patients. (E) Top pathways predicted to be activated (z-score >1) or inhibited (z-score <-1) inferred from 386 significant protein alterations ($p<0.01$) between NACT-ER (n=30) and NACT-PR (n=29) patients. (F) Differential analyses revealed 59 phosphosites significantly altered (adj. $p<0.05$) between NACT-ER (n=17) and NACT-PR (n=22) patients. Heatmap reflects clusters assembled by Pearson correlation and average linkage of significant phosphosite abundance trends. (G) Principle component analyses of 59 phosphosites significantly altered (adj. $p<0.01$) between NACT-ER (n=17) and NACT-PR (n=22) patients. (H) Top pathways predicted to be activated (z-score >1) or inhibited (z-score <-1) inferred from 164 phosphosite alterations (adj. $p<0.05$; **Table S4**) between NACT-ER (n=17) and NACT-PR (n=22) patients.

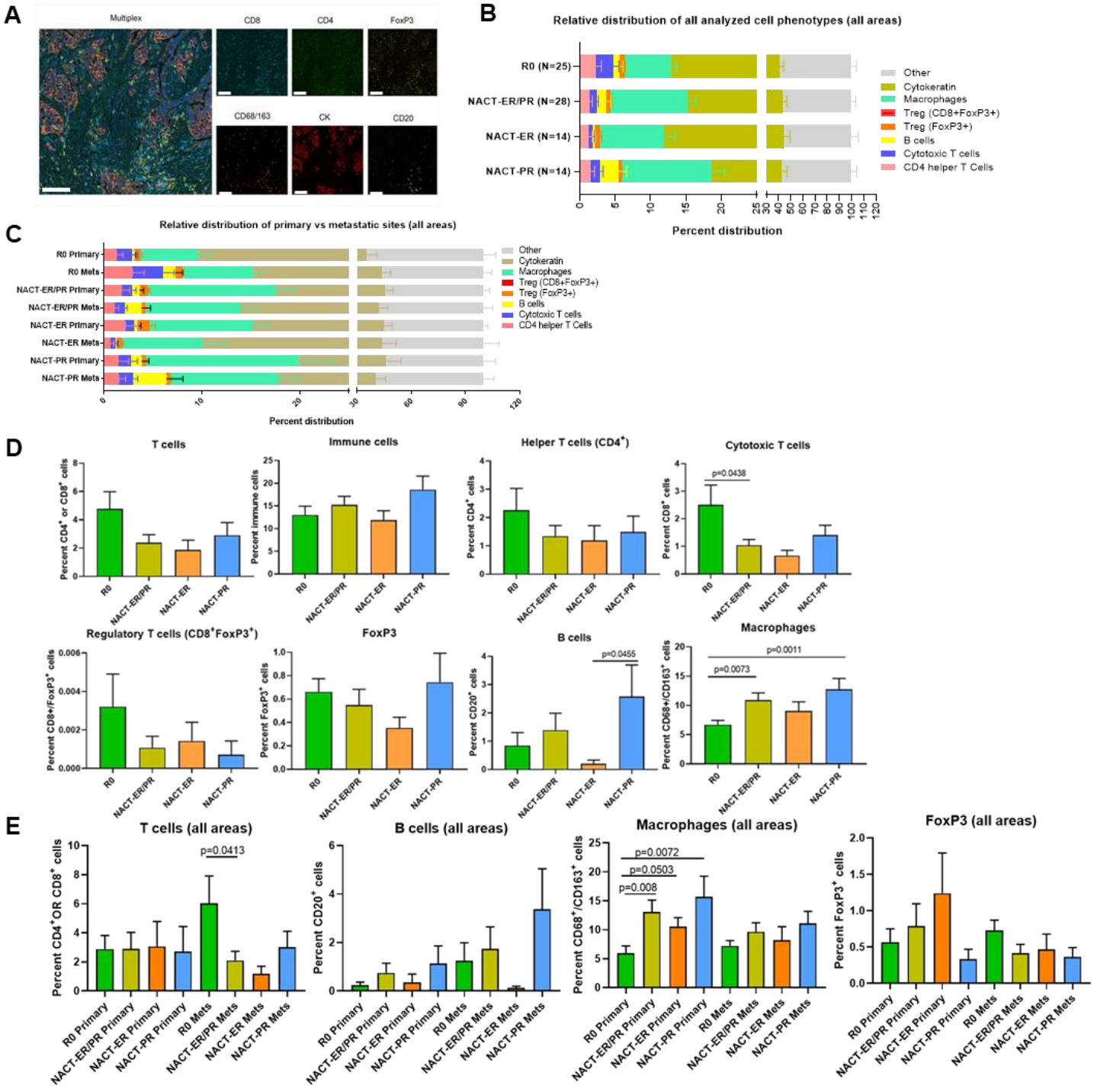

Figure S7. HGSC immune infiltration patterns in all areas (tumor/non-tumor), Related to Figure 4. (A) Opal 7-color multiplex analysis. Representative multiplex images displaying the same multispectral imaging after spectral unmixing, including nuclear marker DAPI (pseudocolored blue), CD8 (membrane, Opal color code 540, pseudocolored cyan), CD4 (membrane, 650, pseudocolored green), FoxP3 (membrane, 570, pseudocolored yellow),

CD68/163 (membrane, 620, pseudocolored orange), cytokeratin (membrane, 690, pseudocolored red), CD20 (membrane, 520, pseudocolored white) and autofluorescence (pseudocolored black; not pictured). (scale bar = 40 µm). (B) Relative distribution of analyzed cell phenotypes in HGSC across the R0, NACT-ER and NACT-PR groups. (C) Relative distribution of immune cell populations separated into primary and metastatic sites in each group. (D) Immune subpopulation infiltration patterns in the R0, NACT-ER and NACT-PR groups. The percentage of immune cells were compared for all T cells, immune cells, helper T cells, cytotoxic T cells, regulatory T cells, macrophages and B cells. Statistical significance was determined by unpaired *t*-test. Data are presented as the mean ± SEM. (E) Immune subpopulation infiltration patterns in primary and metastatic sites. The percentages of T cells, B cells, macrophages, and $FoxP3^+$ cells in all areas (tumor and non-tumor) were compared for each group.

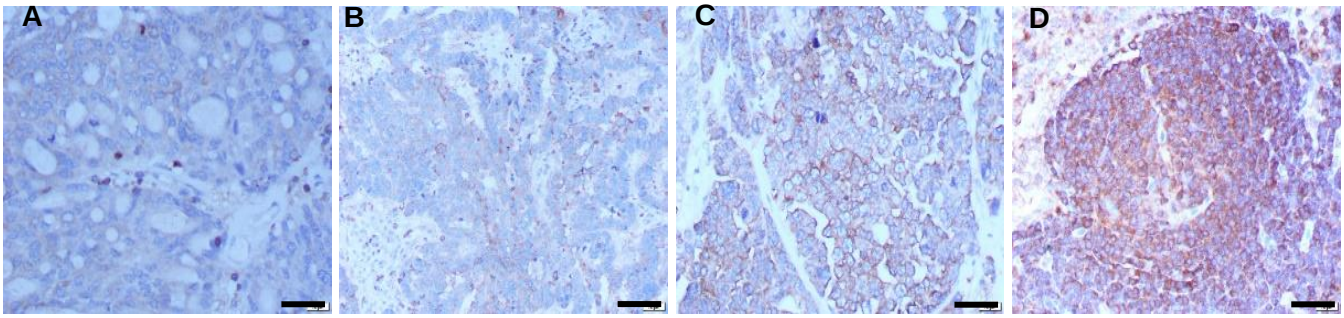

Figure S8. The representative cases of NF1 IHC scores, Related Figure 4. NF1 expression in tumors was scored 0 (negative, A), 1 (weak, B), 2 (mild expression, C), and 3 (strong expression, D) based on the intensity of NF1 IHC staining across the R0, NACT-ER and NACT-PR groups (scale bar = 40 μm).